ENVIRONMENTAL RESEARCH
LETTERS

LETTER • OPEN ACCESS

Spatiotemporal dynamics of encroaching tall vegetation in timberline ecotone of the Polar Urals Region, Russia

To cite this article: Wenbo Zhou *et al* 2022 *Environ. Res. Lett.* **17** 014017

IOP Publishing Environ. Res. Lett. 17 (2022) 014017 https://doi.org/10.1088/1748-9326/ac3694

ENVIRONMENTAL RESEARCH
LETTERS

OPEN ACCESS

RECEIVED
3 June 2021

REVISED
18 October 2021

ACCEPTED FOR PUBLICATION
4 November 2021

PUBLISHED
30 December 2021

LETTER

Spatiotemporal dynamics of encroaching tall vegetation in timberline ecotone of the Polar Urals Region, Russia

Wenbo Zhou[1], Valeriy Mazepa[5], Stepan Shiyatov[5,7], Yulia V Shalaumova[6], Tianqi Zhang[4], Desheng Liu[4], Aleksey Sheshukov[2], Jingfeng Wang[3], Husayn El Sharif[3] and Valeriy Ivanov[1]

[1] Department of Civil and Environmental Engineering, University of Michigan, Ann Arbor, MI, United States of America
[2] Department of Biological and Agricultural Engineering, Kansas State University, Manhattan, KS, United States of America
[3] School of Civil and Environmental Engineering, Georgia Institute of Technology, Atlanta, GA, United States of America
[4] Department of Geography, Ohio State University, Columbus, OH, United States of America
[5] Institute of Plant and Animal Ecology, The Ural Branch of the Russian Academy of Sciences, Yekaterinburg, Russia
[6] Laboratory of Mathematical Modeling in Ecology and Medicine, Institute of Industrial Ecology, the Ural Branch of the Russian Academy of Sciences, Yekaterinburg, Russia
[7] Dr Stepan Shiyatov is deceased.

E-mail: zhouwb@umich.edu and ivanov@umich.edu

Keywords: encroachment, ecotone, patterns, microtopography, snow

Supplementary material for this article is available online

Abstract

Previous studies discovered a spatially heterogeneous expansion of Siberian larch into the tundra of the Polar Urals (Russia). This study reveals that the spatial pattern of encroachment of tree stands is related to environmental factors including topography and snow cover. Structural and allometric characteristics of trees, along with terrain elevation and snow depth were collected along a transect 860 m long and 80 m wide. Terrain curvature indices, as representative properties, were derived across a range of scales in order to characterize microtopography. A density-based clustering method was used here to analyze the spatial and temporal patterns of tree stems distribution. Results of the topographic analysis suggest that trees tend to cluster in areas with convex surfaces. The clustering analysis also indicates that the patterns of tree locations are linked to snow distribution. Records from the earliest campaign in 1960 show that trees lived mainly at the middle and bottom of the transect across the areas of high snow depth. As trees expanded uphill following a warming climate trend in recent decades, the high snow depth areas also shifted upward creating favorable conditions for recent tree growth at locations that were previously covered with heavy snow. The identified landscape signatures of increasing tall vegetation, and the effects of microtopography and snow may facilitate the understanding of treeline dynamics at larger scales.

1. Introduction

The Arctic terrestrial ecosystems have been changing in response to the global warming (Hinzman *et al* 2005) over the past decades. Numerous studies have reported shrubification and tree expansion into tundra ecosystems towards higher latitudes and areas of higher elevation (Sturm *et al* 2001, Tape *et al* 2006, Forbes *et al* 2010, Myers-smith *et al* 2011, Elmendorf *et al* 2012, Frost and Epstein 2014). The process has been proliferating and is well documented for many places in the Arctic from both direct *in situ* observations, dendrochronological analyses (Lloyd and Fastie 2002, Shiyatov *et al* 2007, Devi *et al* 2008, Van Bogaert *et al* 2011, Martin *et al* 2017) and satellite-based observations (Lloyd *et al* 2011, Frost *et al* 2014, Mathisen *et al* 2014). With a warming trend projected for the coming decades, the change of tundra plants at the circumpolar scale is expected to continue in the future (Bjorkman *et al* 2018), including both structural shifts from low to high shrubs or trees (Forbes *et al* 2010, Macias-fauria *et al* 2012) and migration-based treeline advances (Macdonald *et al* 2008, Vavrus *et al* 2012, Koenigk *et al* 2013).

The observed replacement of short tundra vegetation (graminoids, forbs, and non-vascular vegetation) to tall erect woody plants (shrubs and trees) are thought to be induced mainly by increasing temperature (Walker *et al* 2006, Elmendorf *et al* 2012),

along with the impacts of other important drivers like precipitation, soil moisture, snow dynamics, and herbivory (Frost and Epstein 2014, Martin *et al* 2017). This process will likely have positive feedback to climate and enhance warming through changes of albedo, evapotranspiration, and carbon cycle (Lafleur *et al* 2001, Foley *et al* 2003, Chapin *et al* 2005, Pearson *et al* 2013, Zhang *et al* 2013, Lafleur and Humphreys 2018). Furthermore, this process can potentially alter wildlife habitat (Tape *et al* 2016). Forest-tundra boundaries have been found to be temperature-sensitive transitional zones (Esper and Schweingruber 2004, Harsch *et al* 2009). While treeline location is mainly controlled by summer temperatures and growing season length (Macdonald *et al* 2008, Hoch and Korner 2009), treeline advances have also been found to be associated with winter warming (Kullman 2007, Hagedorn *et al* 2014). Although tree growth is considered to be mainly limited by low temperatures (Körner and Paulsen 2004), other environmental conditions also affect tree distribution patterns (Holtmeier and Broll 2005) leading to spatial heterogeneity in treeline advances (Lloyd *et al* 2002, Wilmking *et al* 2004).

The northern Siberian region encompasses the largest forest-tundra ecotone in the world (Frost and Epstein 2014) and exhibits large gradients in summer conditions and regional differences in vegetation distribution (Macdonald *et al* 2008). Previous studies have shown various rates of vegetation expansion across northern Siberia strongly correlated with increased winter precipitation (Frost and Epstein 2014, Devi *et al* 2020). This can be explained by the impact of winter precipitation on soil hydrological and thermal mechanisms. On the one hand, the increase of winter precipitation may provide extra water supply for seedlings and saplings during the growing season (Grigorieva and Moiseev 2018, Devi *et al* 2020); on the other hand, snow cover is essential for new trees to survive along the treeline as snowpack increases soil temperature and protects against frost and wind abrasion stresses (Holtmeier and Broll 2007, Kharuk *et al* 2010a, Hagedorn *et al* 2014). Landscape features also influence the spatial distribution of forests, thereby mediating their response to ambient warming (Kharuk *et al* 2010b, Dearborn and Danby 2018). In the areas of complex topography including mountainous regions, tall vegetation would have higher or lower favorability over different microtopographic niches. This preference of vegetation depends on environmental factors such as slope type and snow redistribution, which can lead to spatially varying treeline sensitivity to climate (Holtmeier and Broll 2005). Topography-mediated hydrological conditions such as drought and flooding stresses can also affect the boreal forest response to climate at regional scales (Sato and Kobayashi 2018). Soil nutrient is also a key player in biomass dynamics if the low-temperature limitation of tree growth at the treeline starts weakening in the future (Hagedorn *et al* 2020). An emerging question is: as the climate is becoming less limiting for the encroachment of tall vegetation, are there other appreciable factors controlling the distribution of trees over the forest-tundra ecotone?

This study aims to analyze spatiotemporal patterns of the larch forest encroachment into tundra and relevant environmental factors with a focus on two features: microtopography and snow cover. We analyze the timberline ecotone in the Polar Urals region where a unique set of records on tree growth dynamics along with environmental features data are available since the 1960s. The 'timberline ecotone' refers to a transitional belt of mountain vegetation between the upper limit of closed forests and the upper limit of single tree growth in the tundra (Körner 2003, Shiyatov *et al* 2005). We hypothesize that the spatiotemporal pattern of tree distribution of this ecotone is associated with niches of favorability caused by microtopography and snow cover.

2. Materials and methods

2.1. Study site and vegetation

The study region of the Rai-Iz massif is located on the eastern slope of the Polar Urals range (200–350 m asl.), in the Sob' River watershed (ca. 66°46′ N, 65°49′ E) underlain by the continuous permafrost (figures 1(a) and (c)). The bedrock is mainly comprised of Paleozoic amphibolite and crystal granodiorite (Mazepa *et al* 2011). The most common soil in the Polar Urals is mountain-tundra gleysol, and rare inclusion of mountain-tundra turf soils. On the ultramafic massif of Rai-Iz, soils are characterized by neutral and near-neutral pH (Kataeva *et al* 2004). According to data collected at Salekhard meteorological station (55 km southeast of the study area, 35 m asl.) between 1883 and 2005., the mean annual, mean monthly minimum (January) and maximum (July) air temperatures are −6.7°, −24.4°, and 13.8 °C, respectively. The mean annual precipitation is 600 mm with 50% as snow and sleet. The growing season lasts from mid-June to earlyAugust with a mean frost-free period of 94 d. Westerly wind prevails, while northeasterly wind is also present in early summer (see S1 available online at stacks.iop.org/ERL/17/014017/mmedia), with an average wind speed of 1–3 m s^{-1} and maximum speed observed during the winter season (Mazepa 2005).

Starting in the early 1960s, six permanent altitudinal transects of 300–1100 m long and 20–80 m wide were established in the eastern foothills of the mountain range for long-term monitoring of spatiotemporal dynamics of alpine forest-tundra and forest-meadow communities. Transects typically start at the upper timberline boundary, where live trees are not yet present, and extend down into the upper limit of closed forest (Mazepa *et al* 2011). This study

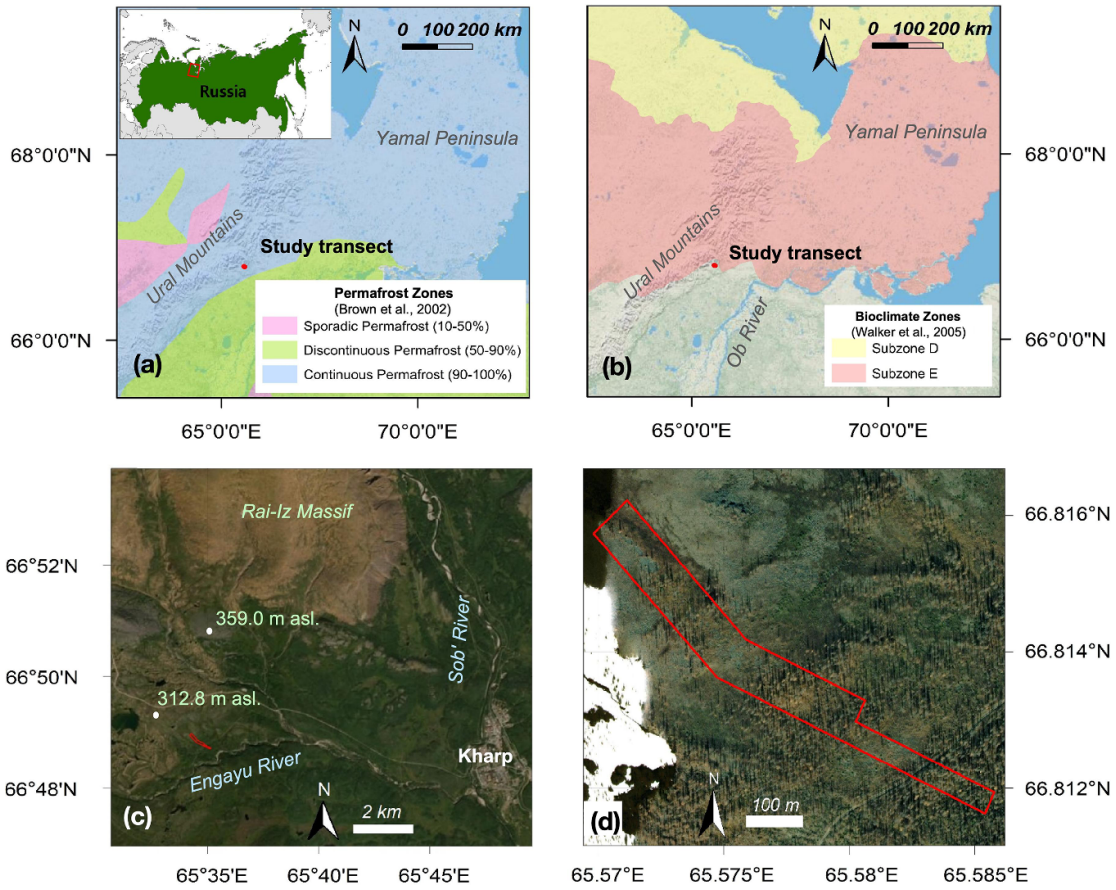

Figure 1. Maps of the study area: (a) the permafrost zones (Brown *et al* 2002) and (b) the bioclimate subzones (Walker *et al* 2005 in the Polar Urals region. (c) The vicinity of the Rai-Iz massif and the Sob' river watershed, where the studied transect (red polygon) is located. Elevations of hilltops near the transect have been displayed. (d) Outline of the studied transect. The permafrost zones in (a) are classified based on the percentage (as in the legend) of landscape underlain by permafrost. In (d), elevation ranges from 194 (bottom-right) to 257 (top-left) m asl.

focuses on the earliest ecotone transect within which complete data of tree characteristics, terrain elevation, and snow distribution have been collected for multiple years (figure 1(d)). This transect also exhibits varying topography, as compared to the other transects. The transect is 860 m long and 40–80 m wide (the total area is 5.6 ha, with the upper left corner at 66°48′57″ N, 65°34′09″ E) and oriented along the direction of the predominant westerly wind (Mazepa 2005, Shiyatov and Mazepa 2011).

This transect is located close to the southern boundary of the bioclimate subzone E (Walker *et al* 2005) as shown in figure 1(b). Tree stand composition within the timberline ecotone is relatively simple: larch (*Larix sibirica* Ledeb.) forest-tundra communities dominate in the upper part, while open larch forest with Siberian spruce (*Picea obovata* Ledeb.) and downy birch (*Betula tortuosa* Ledeb.) occur in the lower part of the area (Shiyatov *et al* 2005). Dwarf birch (*Betula nana* L.) is abundant in the lower and middle parts of the transect. Names of plant species correspond to the Integrated Taxonomic Information System (ITIS 2021). Historically, boreal trees grow at the fringe of the forest-tundra ecotones in various growth forms (creeping, prostrate, single-stemmed, and multi-stemmed), which reflect adaptations to environmental changes (Mazepa and Devi 2007, Devi *et al* 2008). Over 90% of the young trees appearing in the study transect after 1950 are single-stemmed (Mazepa *et al* 2011). The studied forest stands, and recent vegetation growth have emerged without significant impacts from reindeer grazing, fire, and human activities (such as logging) over at least the last millennium (Mazepa 2005, Devi *et al* 2020).

2.2. Tree structural and allometric characterization

The records of three census campaigns in 1960, 1999, and 2011 are used in this study to quantitatively assess the changes in the composition, structure, and spatial distribution of the forest-tundra communities. Specifically, detailed mappings of all alive and dead tree locations, measurements of their allometric and geometric characteristics such as height, crown size, branch position, and diameter at multiple heights were produced during these campaigns. All three censuses predominantly recorded larch with the occasional presence of spruce along the study transect. The numbers of trees for the 1960, 1999, and 2011 censuses are 1853, 1700, and 1398, respectively, after pre-screening (see supplementary materials (S2)).

After reconstructing the missing tree diameter data using an allometric function (see S2), we compute the change of tree diameters ΔD between censuses as the proxies for the increase of biomass and tree productivity, and then relate them to environmental features. Specifically, to compare changes of tree diameters ΔD for different periods (i.e. from 1960 to 1999, and from 1999 to 2011), the relative diameter change $\Delta D_{\mathrm{rel}} = \Delta D/D_0$, where D_0 is the tree diameter at the first year of the corresponding period, is computed first. ΔD_{rel} is then normalized by the period of time T (years) to get the annual relative change rate of stem diameter $\dot{D}_{\mathrm{rel}} = \sqrt[T]{1+\Delta D_{\mathrm{rel}}} - 1$ assuming a constant annual change rate for a given period. This rate was computed only for trees recorded both at the start and end year of the time interval between the two censuses. The changes in tree diameter may also be used as a proxy of tree biomass change through its relationship with sapwood (see S2).

2.3. Snow distribution

Snow data were collected along the study transect in 1961, 2006, and 2013 in the spring, when snow depth (Z_{S}) was at its peak by direct measurement, tree marking, and visual assessment (see S3). The relative snow depth, defined as $\hat{Z}_{\mathrm{S}} = (Z_{\mathrm{S}} - Z_{\mathrm{Smin}}) / (Z_{\mathrm{Smax}} - Z_{\mathrm{Smin}})$ where Z_{Smax} and Z_{Smin} are the maximum and minimum snow depths within the transect for a given survey year from the three surveys, is shown in figure 2.

2.4. Topographic analysis

Digital terrain models (DTMs) are needed to capture topography at fine scales, but there are limited areas in the Arctic for which high-resolution DTMs are available. There is a range of digital elevation model (DEM) products that can provide high-resolution elevation maps. However, these DEM products are affected by the presence of surface biomass masking the location of actual topography. To reconstruct the DTM for the transect, we combined a resampled 2 × 2 m resolution grid from a 20 × 20 m regularly spaced field terrain measurements of the transect, and a 2 m resolution DEM product called ArcticDEM (Porter *et al* 2018). After co-registering two ground sources (i.e. field measurement and ArcticDEM), we manually selected bare ground grids from ArcticDEM together with the field measurement to extract a high-resolution DTM for the study transect by natural neighbor interpolation (Tily and Brace 2006).

Terrain curvature is one of the fundamental topographic properties and an important driver of hydrologic processes (Moore *et al* 1991). Two types of curvature indices, i.e. profile curvature and planform curvature defined by the Environmental Systems Research Institute (ESRI 2021), are used to represent micro-topographic features in this study. Specifically, profile curvature is the curvature of the surface in the direction of the steepest slope, while planform curvature is the curvature in the plane perpendicular to the direction of the steepest slope. For profile curvature index, a negative value indicates an upwardly convex or dome-shaped surface, while a positive value represents a concave surface or depression; for planform curvature index, negative and positive values indicate a laterally concave and convex surface, respectively. Note that the opposite sign is used in the definition of planform curvature concavity/convexity to that of profile curvature. In conventional terrain analysis, the curvature indices are calculated from DTM as the second-order derivative of elevation map using various geomorphometric methods (e.g. Zevenbergen and Thorne 1987). The curvature indices calculated from the resampled DTM with various resolutions are used to capture topographical features at different scales (see S4).

To attribute topographic locations to niches of higher or lower favorability for tree encroachment, we computed the weighted average curvature index using stem diameter at locations where trees are present as a weight:

$$\bar{\kappa}_p = \frac{\sum D_i \kappa_{i,p}}{\sum D_i}, \tag{1}$$

where D_i is the diameter of tree i, $\kappa_{i,p}$ is the curvature index of a terrain grid cell where the tree is located, and the summation is for all trees along the transect. The index p represents either planform or profile curvature index. Noted that $\kappa_{i,p}$ as well as the number of trees within a given grid cell change with resolutions, so the summation is not carried out over the same set of trees for different grid resolutions. The above formulation emphasizes the contributions of curvature indices of terrain locations with higher D. The rationale is that stem diameter is argued to be an indicator of biomass and long-term productivity (section 2.2). If there is an enhanced tree growth at topographic locations of specific curvature, it can be elucidated by comparing $\bar{\kappa}_p$ in (1) with the average curvature of transect topography as the arithmetic mean of curvature over all grid cells along the transect at different grid resolutions.

2.5. Stem density clustering analysis

Spatial point pattern analysis is commonly used to characterize the patterns of the spatial distribution of tree species (e.g. Condit *et al* 2000). Most of these analyses use a family of statistics derived from the Ripley's K-function (Ripley 1976) to quantify the species clumping characteristics by comparing them with complete spatial randomness (CSR). In this study, following the approach proposed by Plotkin *et al* (2002), we apply a density-based spatial clustering method with the presence of noise (i.e. points located too far from other points) (Ester *et al* 1996) to capture

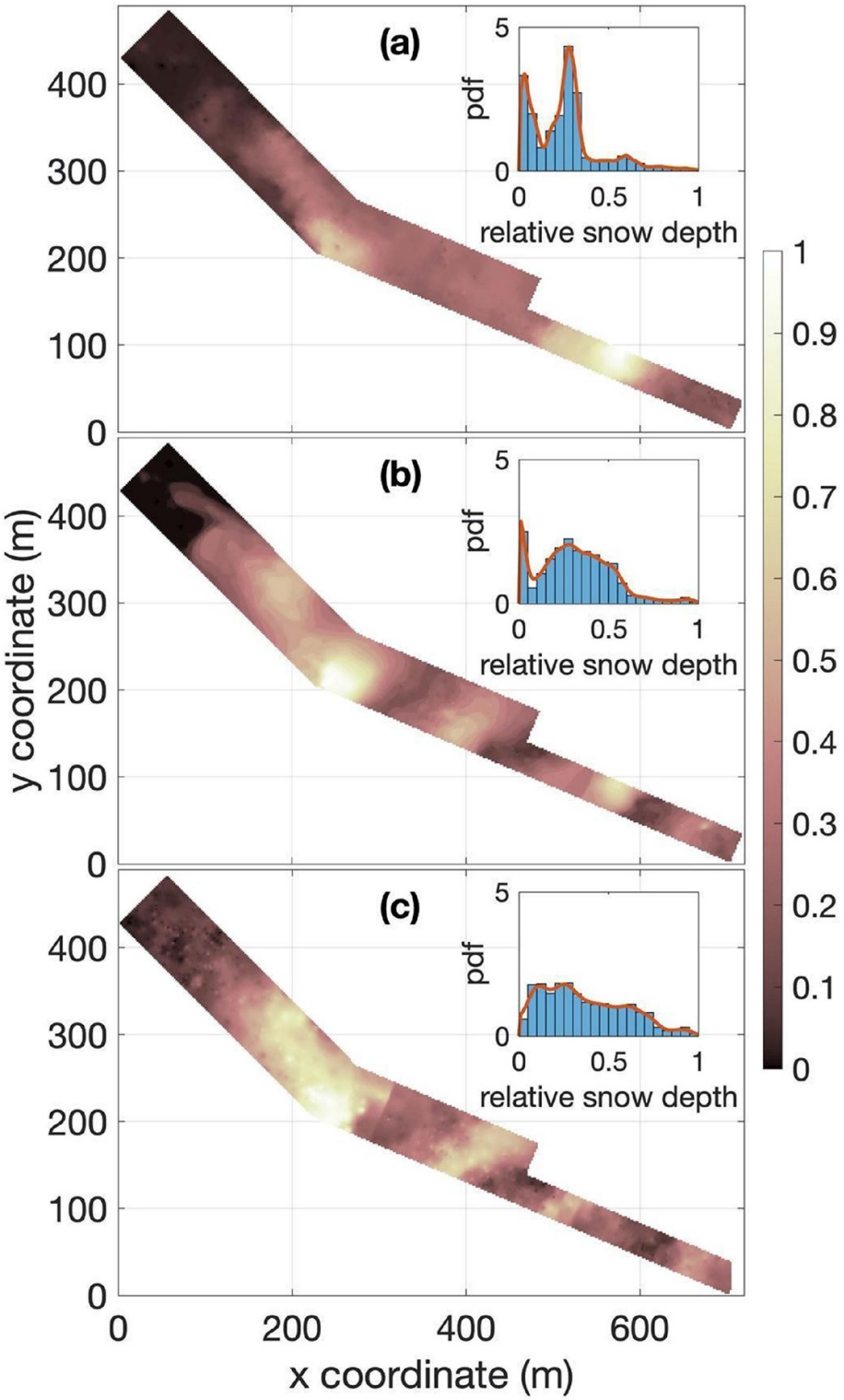

Figure 2. The spatial distribution of the relative snow depth in the study transect in 1961 (a), 2006 (b), and 2013 (c). Plot insets show the relative density (bars) and the probability density function of the relative snow depth estimated with kernel density (red curves in the insets) using a Gaussian kernel. The transect was mapped to a relative coordinate frame, where the *x* and *y* axes align with the lowermost and leftmost point of the transect, respectively.

spatial pattern of tree distribution. The advantage of this method is that it does not require *a priori* number of clusters, such as in k-means analysis (Macqueen 1967), and can identify clusters of arbitrary shape. Clusters of tree locations (referred to as 'points') are derived at different spatial resolutions using the records of the three tree censuses (section 2.2). The algorithm requires two parameters: neighborhood search radius (d) and the minimum number (q) of points required to form a cluster located within the search radius. By setting the parameter q to 1 in all analyses, we make the clustering process depend only

on the parameter d, which thus represents the maximum distance between any pair of connected trees belonging to the same cluster. Therefore, for any given value of d all stem locations are partitioned into a unique set of clusters.

Tree clusters were formed at different spatial scales by changing the parameter d from 0 to the maximum distance between locations of any two connected trees in the transect (65 m). For a given d, the total number of obtained clusters is denoted as m and the size of an ith cluster as c_i. The sample size, i.e. the total number of trees in the transect, is denoted as $n = \sum_{i=1}^{m} c_i$. The unique arrangement of clusters for a specific value of d can be summarized with the normalized mean cluster size:

$$\hat{c} = \frac{1}{n^2} \sum_{i=1}^{m} {c_i}^2. \quad (2)$$

This variable represents the probability that two randomly chosen tree locations belong to the same cluster (Plotkin *et al* 2002). For example, $\hat{c} = 1/n$ when $d = 0$, corresponds to a clustering pattern that each point forms its own cluster; $\hat{c} = 1$ when d equals the maximum pairwise distance between any two connected tree locations, i.e. all trees form a single cluster. The clustering pattern varies for intermediate values of d and can be obtained by recording the concomitant change of $\hat{c}$, known as the mean cluster size curve $\hat{c}(d)$. To make the results for censuses with different sample sizes comparable in the mean cluster size curves, we use the normalized distance $\hat{d}$ defined as

$$\hat{d} = d\sqrt{n/A}, \quad (3)$$

where A is the transect area. Spatial patterns of clustering can then be compared with CSR (see S5).

3. Results

3.1. Stem diameter change

The sampling distribution of the annual relative change rate of stem diameter $\dot{D}_{\mathrm{rel}}$ for the two periods between the three censuses, (1960–1999 and 1999–2011) is shown in figure 3(a). The mode of the distribution increased from 2%/year to 3%/year, indicating accelerated growth in the later period. The right-skewed distribution of the second period implies that the proportion of trees with higher growth rates is larger in the recent period. Figure 3(b) shows the relationship between $\dot{D}_{\mathrm{rel}}$ and D_0 for the two periods between the three field surveys. The maxima of $\dot{D}_{\mathrm{rel}}$ form a clear upper boundary with respect to D_0 for both periods, indicating the upper limit of the annual growth rate and the results illustrate an increase of these growth rates from the earlier to the later period (red and blue lines). The highest growth rate decreasing with D suggests that larger, older trees grow slower than smaller, younger trees. Growth rates can vary significantly, between just above zero and to a few percent of their stem diameter per year.

3.2. Tree locations and terrain curvature indices

Figure 4 compares the average, D-weighted terrain curvature index for grid cells with live trees (equation (1)) and the transect average index (i.e. uses all grid cells), as a function of DTM grid cell resolution. The results indicate scale-dependent differences with respect to the transect average for both planform and profile curvatures, and for all censuses. The difference is significant for DTM grid sizes ranging from 2 to 14 m, with the largest difference occurring at the grid size of 10 m. This implies the preference of tree growth in terrain curvature is characterized most significantly at this scale (i.e. 25–30 m length scale of landforms, which is the size of the moving window used to compute the curvatures, see S4). At locations with live trees, the profile curvature index is more negative, and the planform curvature index is more positive than the overall transect averages, implying that trees tend to cluster at sites with convex topography. The curvatures of the locations with trees and the transect average become indistinguishable for grid cells of sizes greater than 14 m. Since the number of grids along the transect decreases with grid size, this leads to the convergence of the curvature indices to the same value.

3.3. Tree cluster dynamics

The resultant cluster size curves for the three censuses are shown in figure 5. The sharp transitions in the three curves at various distances $\hat{d}$ (equation (3)) correspond to the 'continuum percolation' phenomenon (Meester and Roy 1996, Plotkin *et al* 2002), i.e. the aggregation of isolated smaller clusters into a larger cluster. The corresponding distance is known as the 'critical distance' or 'percolation threshold'. When $\hat{d}$ is below the threshold, elements in the system of interest are disconnected and form many smaller-sized clusters; above the percolation threshold, the elements are aggregated to form larger clusters. In theory, for true CSR (i.e. if the sample size is infinitely large) the cluster size curve will show a discontinuous transition corresponding to the step function at a critical distance of $\hat{d} \approx 1.2$ (an abrupt transition for the developed CSR curve in figure 5 is not discontinuous due to the finite sample size and transect edge effects on the computation of $\hat{d}$).

The cluster size curves constructed using the actual tree locations from all censuses have three transitions at varying critical distance $\hat{d}$. Their differences with respect to the CSR curve imply a non-random spatial tree distribution at different spatial scales. The plateaus of the curves between the abrupt transition in cluster sizes represent the ranges of d within which the change of cluster pattern is insignificant. The number of plateaus (two

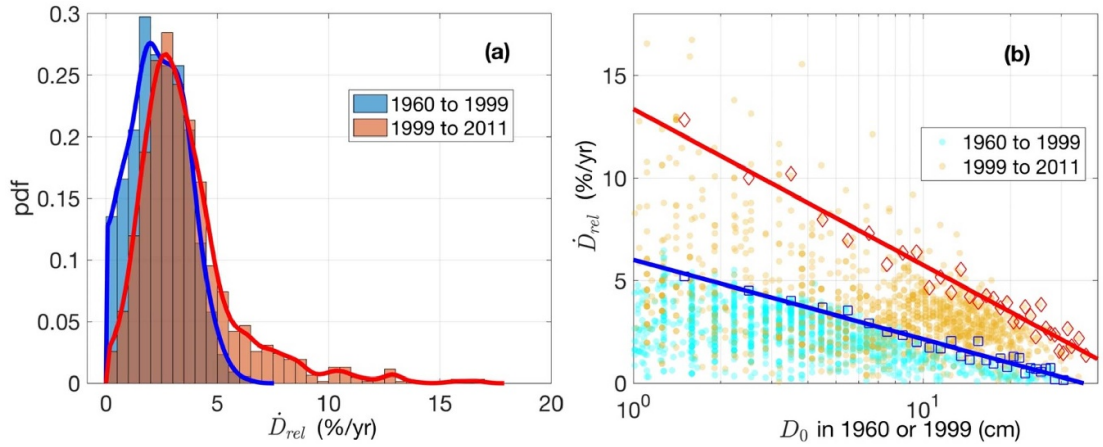

Figure 3. (a) The sampling probability density function (pdf) of the annual relative rate of stem diameter change, $\dot{D}_{\mathrm{rel}}$ (a proxy for stem growing rate), for the two periods between field surveys: from 1960 to 1999, and 1999–2011. The blue and red curves are the probability density functions estimated using a Gaussian kernel for 1960–1999 and 1999–2011, respectively. (b) A relationship between the $\dot{D}_{\mathrm{rel}}$ from 1960 to 1999 (cyan dots) and 1999–2011 (orange dots) and the stem diameter at the start year (D_0) for each period. The logarithmic scale is used for the horizontal axis. Blue (1960–1999) and red (1999–2011) lines are the upper boundaries of the change rate. To construct the boundaries, we calculated 95% percentiles of $\dot{D}_{\mathrm{rel}}$ for bins of D_0 (plotted as blue squares and red diamonds) and a linear regression with respect to $\log(D_0)$ at the center of each bin was fitted.

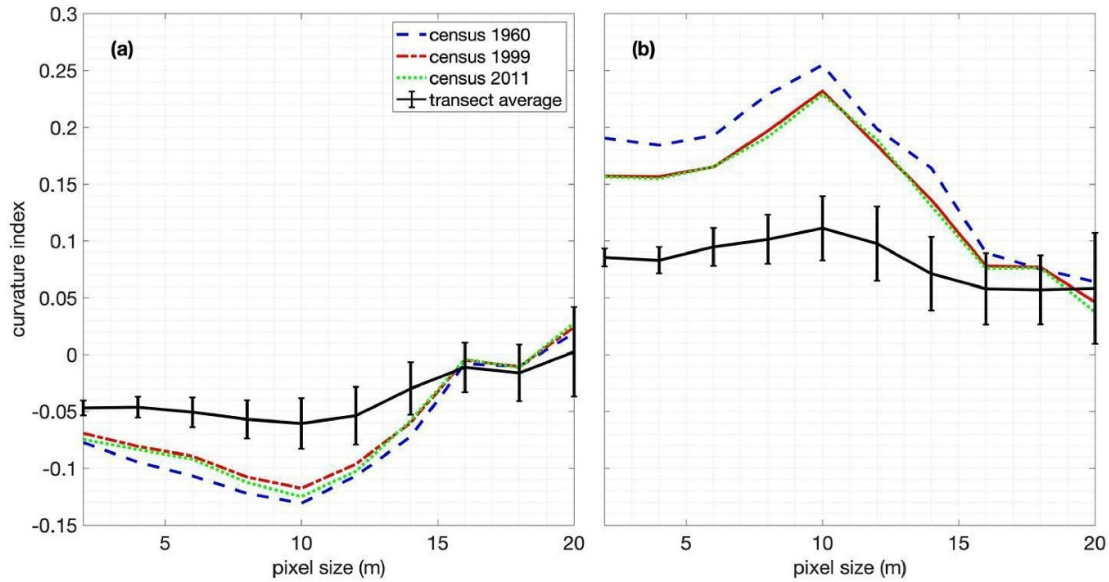

Figure 4. Transect curvature indices as a function of the DTM resolution: (a) average profile curvature index and (b) average planform curvature index computed over all locations with live trees, all censuses (colored curves), for different grid cell sizes. Averaged curvature indices estimated using all grids in the transect are shown with black lines; whiskers represent the 95% confidence interval.

for this case) indicates the number of scales of non-random aggregation (Plotkin *et al* 2002). Therefore, one may perform a clustering analysis using d corresponding to a plateau region to represent such a stable distribution at a selected scale. Here we choose the values of normalized distance corresponding to the start of plateaus immediately after the occurrence of 'continuum percolation'. The following clustering analysis uses $\hat{d}$ corresponding to the first plateaus ($\hat{d}_1$) in figure 5: 1.24, 1.4, and 1.51 (i.e. the actual distances are $d_1 = 6.7$, 7.9, and 9.4 m) for the 1960, 1999, and 2011 censuses, respectively. For the second plateau ($\hat{d}_2$) in figure 5, the normalized distances are $\hat{d}_2 = 2.37$, 3.63, and 5.58 ($d_2 = 12.8$, 20.5, and 34.7 m). When a cluster pattern corresponding to $\hat{d}_1$ is defined as the 'primary cluster set', then the value of $\hat{d}_1$ is a representative proxy of the distance among trees within any cluster of this set, while $\hat{d}_2$ represents a proxy of the distance between borders of clusters formed by the primary set. As figure 5 shows, over time relatively smaller changes of the distribution pattern occurred within the primary cluster set, as reflected by the comparable magnitudes of $\hat{d}_1$ across the three censuses. The distances between the

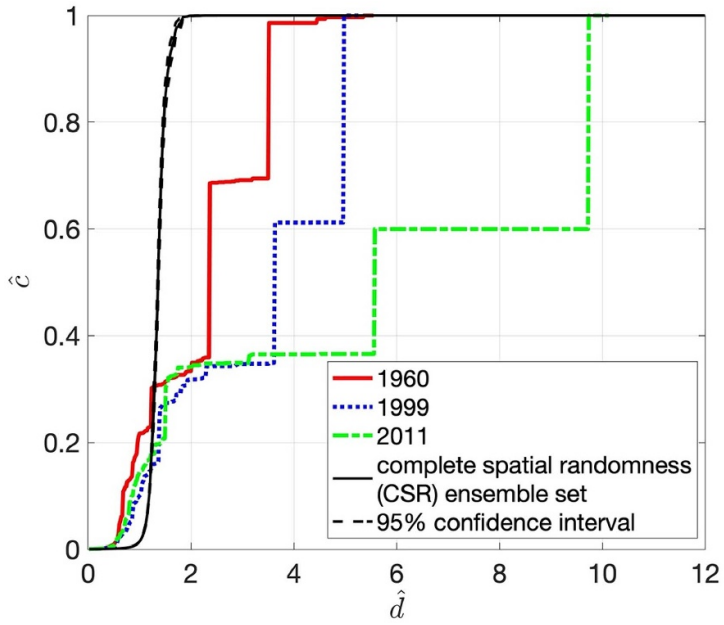

Figure 5. Normalized mean cluster size curves for the three censuses (colored lines) and the complete spatial randomness (CSR) ensemble set. The CSR curve (black solid line) shows the curve averaged over 1000 members of the CSR ensemble set; the black dashed curves represent the 95% confidence interval for this set. The normalized mean cluster size, $\hat{c}$, represents the probability that two randomly chosen tree locations fall in the same cluster. While $\hat{d}$ is the normalized maximum pairwise distance between two connected tree locations (see text for details). The plateaus of the curves between the abrupt transition in cluster sizes represent the ranges of $\hat{d}$ within which the change of cluster pattern is insignificant. The $\hat{d}$ corresponding to the start of plateaus is the critical distance.

cluster borders however become larger, as illustrated by the increase of $\hat{d}_2$, particularly for the census of 2011 (mainly due to the mortality of trees at cluster borders).

Figure 6 shows the spatial distributions of tree clustering for the two critical distances $\hat{d}$. Transitions of cluster patterns can be detected by comparing plots in the same row. For example, when the distance changes from $d_1 = 6.7$ m to $d_2 = 12.8$ m (the census of 1960), the number of clusters decreases significantly from 102 to 21 due to cluster aggregation. The same 'continuum percolation' phenomenon is observed for the other census data of 1999 and 2011. Comparing plots in the same column reveals that the number of primary clusters decreases over time. This phenomenon can be explained by the disappearance of cluster 'noise', i.e. those trees that form their own cluster. Notice that for the primary cluster set (the left panel of figure 6), the sum of cluster sizes of the three largest clusters is over 80% of the total number of surveyed trees (not shown).

Figure 7 illustrates the temporal change of the distribution of the largest cluster from 1960 to 2011. In 1960, there were many small trees scattered in this cluster and larger trees were mainly located in the middle part. A large fraction of small trees previously located in the lower part disappeared in later years, while those in the upper part grew bigger and likely seeded new trees that appeared in the transect in 2011.

Concurrently with the change of the tree distribution pattern, the area with high snow depth had shifted from the lower part to the middle part of this cluster. Similar transitions of areas with high snow depth are also apparent in the regions outside of this cluster (not shown). The area of high snow accumulation shifted from the lower part to the middle-upper part of the transect, coinciding with the growth and densification of trees in clusters at the top.

4. Discussions

Forest expansion in the Polar Urals region is thought to be induced by the increased summer temperature and winter precipitation (Shiyatov *et al* 2005, Devi *et al* 2008, 2020). Analyses of treeline dynamics are usually based on repeated landscape photographs and remotely sensed imagery (Kharuk *et al* 2006, Beck and Goetz 2011, Frost and Epstein 2014), dendrometric survey on tree remnants (Briffa *et al* 2008, Shiyatov and Mazepa 2011, 2015), and treeline models (Kaplan and New 2006, Paulsen and Körner 2014). However, long-term records of allometric characteristics of living trees, as well as snow distribution back to the beginning of the satellite era are rare at tree stand level. This study analyzed spatiotemporal characteristics of the encroachment process of Siberian larch into timberline ecotone of Polar Urals between 1960 and 2011. The unique data sets spanning over 50 years allowed us to carry out tree-level characterizations of landscape favorability for the encroachment process and other features of tree expansion.

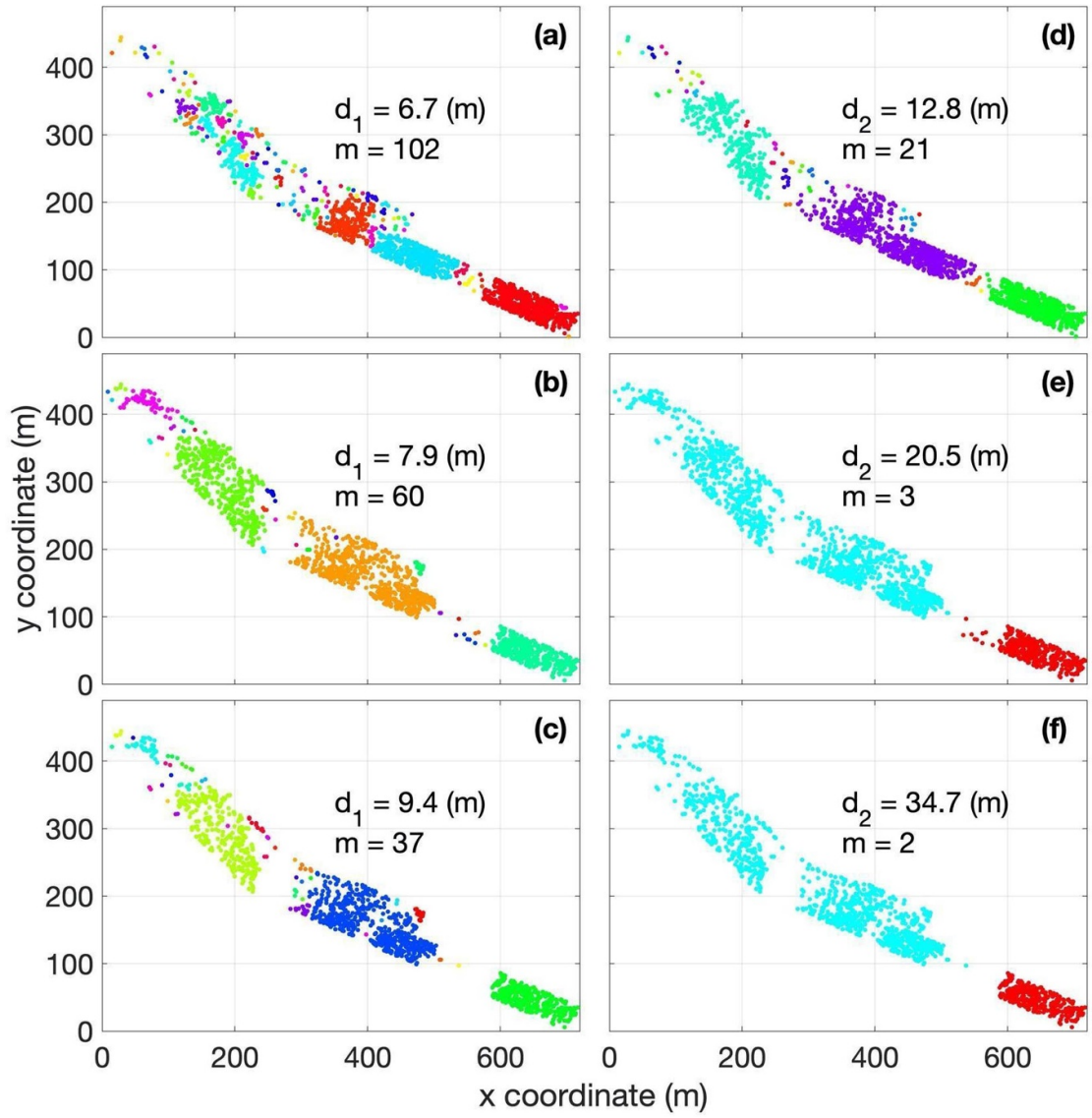

Figure 6. Spatial representation of tree clusters corresponding to the two critical distances $\hat{d}_1$ (left panel, the first critical distance in figure 5, the actual distance is d_1) and $\hat{d}_2$ (right panel, the second critical distance in figure 5, the actual distance is d_2); m is the corresponding number of clusters. The first, second, and third row corresponds to the censuses in 1960, 1999, and 2011, respectively. Circles represent tree locations and each cluster is plotted with a unique color.

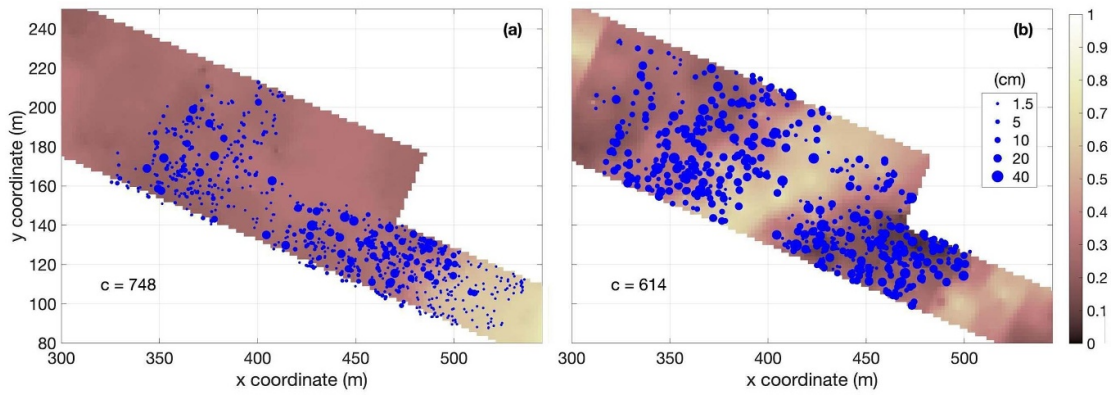

Figure 7. Change of spatial pattern of the largest tree cluster (blue circles) identified for the first 'percolation threshold' in figure 6 (left panel) in (a) 1960 and (b) 2011. Circle sizes are scaled by the tree diameters. The color map indicates the distribution of relative snow depth $\hat{Z}_S$ in (a) 1961 and (b) 2013. Letter 'c') in the panels denotes the cluster size, i.e. the number of trees within this cluster.

Various factors influence the spatial distribution of trees in the timberline ecotone. Considering the small scale of this study that spans a ~1 km-long gentle mountain hillslope, climatic factors such as temperature and precipitation as well as topographic features such as elevation and slope aspect are relatively uniform along the transect. In spite of the spatially homogeneous climate, our analysis reveals a consistent signature of terrain favorability with respect to the curvature indices derived from the data for all censuses. Trees tend to grow on convex or 'bulged' surfaces along the study transect, indicating the preference of trees to be located at sites with divergent surface characteristics. Considering topographic features as proxies for hydrologic dynamics, these locations correspond to well-drained sites. Convex topography may also have negative effects on tree growth, such as extreme windswept and the likelihood of summer drying, impacting seedling establishment (Holtmeier and Broll 2005). The preference of terrain locations with convex curvature is an overall outcome of local-scale hydrologic dynamics combined with more favorable climate conditions (e.g. increasing winter precipitation), dominating over concomitant disadvantages. The subsurface conditions are also important factors affecting tree distribution. Grigorieva and Moiseev (2018) have pointed out the importance of soil moisture on the survival and growth of larch seedlings. Shiryaev *et al* (2019) presented a strong correlation between larch forest advance and increase of soil thaw depth and soil microbiota activities. However, such data are currently unavailable and extremely laborious to collect in the field. Future work augmenting terrain data with soil textural analysis and characterization of the subsurface thermal state is needed.

An increase in the maximum stem growth rate during the most recent period has been observed in this study. Such an increase is expected as the climate warms and the environment becomes more favorable for tree growth, as had been inferred from long-term dendrochronology studies (Briffa *et al* 2008, 2013), field measurements (Devi *et al* 2008), as well as remotely sensed Normalized Difference Vegetation Index analysis (Zeng *et al* 2013, Berner *et al* 2020). The variation in growth rates can be explained by the influence of multiple environmental factors such as soil moisture (Myers-smith *et al* 2015, 2020), soil nutrient availability and non-homogeneity of subsurface freeze-thaw processes (e.g. Sullivan *et al* 2015) for trees located at different locations. Quantitative assessment of their contributions is the topic of future research.

This study shows a clear interaction between changes in spatial patterns of tree locations and the snow distribution shifts. Many small trees and saplings of the largest cluster died between 1960 and 1999 (section 3.2) likely caused by high snow accumulation due to the wind drift—a phenomenon well pronounced at the field transect. Specifically, when snow is redistributed by wind, high roughness obstacles such as trees reduce wind speed at their lee sides leading to leeward snow accumulation (Hiemstra *et al* 2002). In 1960, this accumulation was observed at the bottom of the largest cluster (figure 7(a)). Although snow cover corresponds to a favorable microclimate (Hagedorn *et al* 2014), excessive snow accumulation results in a longer snowmelt period and a shorter growing season reducing total photosynthetic carbon gain and survival chances for small trees. As trees grew and became larger at locations with snow depths that did not limit the duration of the growing season (e.g. the upper part of the largest cluster), the leeward snow accumulation moved towards upslope (figure 7(b)). The increased tree presence in the upper areas in 2011 resulted in a new area of high snow accumulation in the middle part of the cluster. Such a change in surface roughness condition likely made the lower part of the transect even more favorable for trees to grow as indicated by a large number of new stems growing in the lower part. Such growth patterns at different locations with a phase shift signal the effect of spatial teleconnection. This effect has been displayed within and among clusters through interactions between new tree growth and snow distribution changes, which partially explain the heterogeneity of trees encroaching upslope areas along this mountain transect. Since snow distribution can change drastically between consecutive years, one obvious limitation is the incompleteness of the snow record. Improved understanding of the spatial interactions of snow with the tree encroachment process requires a more continuous record of snow distribution at fine-scale resolutions (i.e. at ~1 m).

Treeline is considered a critical indicator of climate warming (Harsch and Bader 2011). Forest extent is predicted to increase 55% in the Arctic with a 42% decrease in tundra area under projected warming in the next few decades (Kaplan and New 2006). The spatial variability of tree expansion, however, indicates the importance of other drivers of vegetation shifts besides summer warming (Elmendorf *et al* 2012). The results presented in this study imply the necessity to take microtopography and snow conditions into account when predicting future timberline ecotone dynamics. Specifically, two thresholds of snow depth need to be determined as a prior: the lower limit, above which trees can survive winter stresses such as wind abrasion and frost, and the upper limit, under which the growing season is long enough for trees to grow. Admittedly, however, these challenges are difficult to overcome as snowpack modeling can be a major source of error in treeline dynamics models due to the lack of precipitation data in mountain or remote regions (Paulsen and Körner 2014). The complexities displayed in the interaction between trees and snow distribution implies that until

this dynamic process approaches a steady state, prediction of treeline dynamics at regional scales will remain difficult and subject to uncertainties.

Data availability statement

The data that support the findings of this study are available upon request from the authors.

Acknowledgments

This research is sponsored by the National Science Foundation Office of Polar Programs grants 1725654 (University of Michigan), 1724868 (Kansas State University), 1724633 (Georgia Tech), and 1724786 (Ohio State University), respectively. V Ivanov and V Mazepa acknowledge the support from project RUB1-7032-EK-11 funded by the U.S. Civilian Research & Development Foundation. V Mazepa acknowledges the partial support from grant RFBR-19-05-00756 from the Russian Foundation for Basic Research. Assistance of Yuriy Trubnikov with data collection and developing allometric relationship is greatly appreciated. The authors thank the two anonymous reviewers for their valuable comments that greatly improved this manuscript.

ORCID iDs

Wenbo Zhou https://orcid.org/0000-0003-4010-1466
Yulia V Shalaumova https://orcid.org/0000-0002-0173-6293
Tianqi Zhang https://orcid.org/0000-0003-0967-0599
Desheng Liu https://orcid.org/0000-0002-6088-5985
Aleksey Sheshukov https://orcid.org/0000-0002-4842-908X
Jingfeng Wang https://orcid.org/0000-0002-2548-6372
Husayn El Sharif https://orcid.org/0000-0003-3146-3844
Valeriy Ivanov https://orcid.org/0000-0002-5208-2189

References

Beck P S and Goetz S J 2011 Satellite observations of high northern latitude vegetation productivity changes between 1982 and 2008: ecological variability and regional differences *Environ. Res. Lett.* **6** 045501

Berner L T *et al* 2020 Summer warming explains widespread but not uniform greening in the Arctic tundra biome *Nat. Commun.* **11** 4621

Bjorkman A D *et al* 2018 Plant functional trait change across a warming tundra biome *Nature* **562** 57–62

Briffa K R, Melvin T M, Osborn T J, Hantemirov R M, Kirdyanov A V, Mazepa V S, Shiyatov S G and Esper J 2013 Reassessing the evidence for tree-growth and inferred temperature change during the Common Era in Yamalia, northwest Siberia *Quat. Sci. Rev.* **72** 83–107

Briffa K R, Shishov V V, Melvin T M, Vaganov E A, Grudd H, Hantemirov R M, Eronen M and Naurzbaev M M 2008 Trends in recent temperature and radial tree growth spanning 2000 years across northwest Eurasia *Phil. Trans. R. Soc. Lond.* B **363** 2271–84

Brown J, Ferrians O, Heginbottom J A and Melnikov E 2002 *Circum-Arctic Map of Permafrost and Ground-Ice Conditions, Version 2* (Boulder, CO: NSIDC: National Snow and Ice Data Center) (https://doi.org/10.7265/skbg-kf16) (Accessed 21 February 2021)

Chapin F S 3RD *et al* 2005 Role of land-surface changes in arctic summer warming *Science* **310** 657–60

Condit R *et al* 2000 Spatial patterns in the distribution of tropical tree species *Science* **288** 1414–8

Dearborn K D and Danby R K 2018 Topographic influences on ring widths of trees and shrubs across alpine treelines in southwest Yukon *Arct. Antarct. Alp. Res.* **50** e1495445

Devi N M, Kukarskih V V, Galimova A A, Mazepa V S and Grigoriev A A 2020 Climate change evidence in tree growth and stand productivity at the upper treeline ecotone in the Polar Ural Mountains *For. Ecosyst.* **7** 7

Devi N, Hagedorn F, Moiseev P, Bugmann H, Shiyatov S, Mazepa V and Rigling A 2008 Expanding forests and changing growth forms of Siberian larch at the Polar Urals treeline during the 20th century *Glob. Change Biol.* **14** 1581–91

Elmendorf S C *et al* 2012 Plot-scale evidence of tundra vegetation change and links to recent summer warming *Nat. Clim. Change* **2** 453–7

Esper J and Schweingruber F H 2004 Large-scale treeline changes recorded in Siberia *Geophys. Res. Lett.* **31** L06202

ESRI. 2021 *Curvature Function* (available at: https://desktop.arcgis.com/en/arcmap/10.7/manage-data/raster-and-images/curvature-function.htm) (Accessed 26 May 2021)

Ester M, Kriegel H P, Sander J and Xu X 1996 A density-based algorithm for discovering clusters in large spatial databases with noise *Kdd* pp 226–31

Foley J A, Costa M H, Delire C, Ramankutty N and Snyder P 2003 Green surprise? How terrestrial ecosystems could affect earth's climate *Front. Ecol. Environ.* **1** 38–44

Forbes B C, Fauria M M and Zetterberg P 2010 Russian Arctic warming and 'greening' are closely tracked by tundra shrub willows *Glob. Change Biol.* **16** 1542–54

Frost G V and Epstein H E 2014 Tall shrub and tree expansion in Siberian tundra ecotones since the 1960s *Glob. Change Biol.* **20** 1264–77

Frost G V, Epstein H E and Walker D A 2014 Regional and landscape-scale variability of Landsat-observed vegetation dynamics in northwest Siberian tundra *Environ. Res. Lett.* **9** 025004

Grigorieva A V and Moiseev P A 2018 Peculiarities and determinants of regeneration of siberian larch on the upper limit of its growth in the urals *Contemp. Problem. Ecol.* **11** 13–25

Hagedorn F, Dawes M A, Bubnov M O, Devi N M, Grigoriev A A, Mazepa V S, Nagimov Z Y, Shiyatov S G and Moiseev P A 2020 Latitudinal decline in stand biomass and productivity at the elevational treeline in the Ural mountains despite a common thermal growth limit *J. Biogeogr.* **47** 1827–42

Hagedorn F, Shiyatov S G, Mazepa V S, Devi N M, Grigor'ev A A, Bartysh A A, Fomin V V, Kapralov D S, Terent'ev M and Bugman H 2014 Treeline advances along the Urals mountain range–driven by improved winter conditions? *Glob. Change Biol.* **20** 3530–43

Harsch M A and Bader M Y 2011 Treeline form–a potential key to understanding treeline dynamics *Glob. Ecol. Biogeogr.* **20** 582–96

Harsch M A, Hulme P E, Mcglone M S and Duncan R P 2009 Are treelines advancing? A global meta-analysis of treeline response to climate warming *Ecol. Lett.* **12** 1040–9

Hiemstra C A, Liston G E and Reiners W A 2002 Snow redistribution by wind and interactions with vegetation at upper treeline in the Medicine Bow Mountains, Wyoming, USA *Arct. Antarct. Alp. Res.* **34** 262–73
Hinzman L D *et al* 2005 Evidence and implications of recent climate change in northern Alaska and other arctic regions *Clim. Change* **72** 251–98
Hoch G and Korner C 2009 Growth and carbon relations of tree line forming conifers at constant vs. variable low temperatures *J. Ecol.* **97** 57–66
Holtmeier F K and Broll G E 2007 Treeline advance-driving processes and adverse factors *Landscape* **1** 1–33
Holtmeier F K and Broll G 2005 Sensitivity and response of northern hemisphere altitudinal and polar treelines to environmental change at landscape and local scales *Glob. Ecol. Biogeogr.* **14** 395–410
ITIS 2021 *Integrated Taxonomic Information System* CC0 (https://doi.org/10.5066/F7KH0KBK) (available at: www.itis.gov) (Accessed 30 September 2021)
Kaplan J O and New M 2006 Arctic climate change with a 2 degrees C global warming: timing, climate patterns and vegetation change *Clim. Change* **79** 213–41
Kataeva M N, Alexeeva-popova N V, Drozdova I V and Beljaeva A I 2004 Chemical composition of soils and plant species in the Polar Urals as influenced by rock type *Geoderma* **122** 257–68
Kharuk V I, Im S T and Dvinskaya M L 2010a Forest-tundra ecotone response to climate change in the Western Sayan Mountains, Siberia *Scandinavian J. Forest Res.* **25** 224–33
Kharuk V I, Ranson K J, Im S T and Vdovin A S 2010b Spatial distribution and temporal dynamics of high-elevation forest stands in southern Siberia *Glob. Ecol. Biogeogr.* **19** 822–30
Kharuk V, Ranson K, Im S and Naurzbaev M 2006 Forest-tundra larch forests and climatic trends *Russ. J. Ecol.* **37** 291–8
Koenigk T, Brodeau L, Graversen R G, Karlsson J, Svensson G, Tjernstrom M, Willen U and Wyser K 2013 Arctic climate change in 21st century CMIP5 simulations with EC-Earth *Clim. Dyn.* **40** 2719–43
Körner C 2003 *Alpine Plant Life: Functional Plant Ecology of High Mountain Ecosystems* 2 (Berlin: Springer) (https://doi.org/10.1007/978-3-642-18970-8)
Körner C and Paulsen J 2004 A world-wide study of high altitude treeline temperatures *J. Biogeogr.* **31** 713–32
Kullman L 2007 Tree line population monitoring of Pinus sylvestris in the Swedish Scandes, 1973–2005: implications for tree line theory and climate change ecology *J. Ecol.* **95** 41–52
Lafleur P M, Griffis T J and Rouse W R 2001 Interannual variability in net ecosystem CO2 exchange at the arctic treeline *Arct. Antarct. Alp. Res.* **33** 149–57
Lafleur P M and Humphreys E R 2018 Tundra shrub effects on growing season energy and carbon dioxide exchange *Environ. Res. Lett.* **13** 055001
Lloyd A H, Bunn A G and Berner L 2011 A latitudinal gradient in tree growth response to climate warming in the Siberian taiga *Glob. Change Biol.* **17** 1935–45
Lloyd A H and Fastie C L 2002 Spatial and temporal variability in the growth and climate response of treeline trees in Alaska *Clim. Change* **52** 481–509
Lloyd A H, Rupp T S, Fastie C L and Starfield A M 2002 Patterns and dynamics of treeline advance on the Seward Peninsula, Alaska *J. Geophys. Res.-Atmos.* **108** ALT 2-1-ALT 2–15
Macdonald G M, Kremenetski K V and Beilman D W 2008 Climate change and the northern Russian treeline zone *Phil. Trans. R. Soc. Lond.*B **363** 2285–99
Macias-fauria M, Forbes B C, Zetterberg P and Kumpula T 2012 Eurasian Arctic greening reveals teleconnections and the potential for structurally novel ecosystems *Nat. Clim. Change* **2** 613–8
Macqueen J 1967 Some methods for classification and analysis of multivariate observations *Proc. Fifth Berkeley Symp. on Mathematical Statistics and Probability* (*Oakland, CA, USA*) pp 281–97
Martin A C, Jeffers E S, Petrokofsky G, Myers-smith I and Macias-fauria M 2017 Shrub growth and expansion in the Arctic tundra: an assessment of controlling factors using an evidence-based approach *Environ. Res. Lett.* **12** 085007
Mathisen I E, Mikheeva A, Tutubalina O V, Aune S and Hofgaard A 2014 Fifty years of tree line change in the Khibiny Mountains, Russia: advantages of combined remote sensing and dendroecological approaches *Appl. Veg. Sci.* **17** 6–16
Mazepa V S 2005 Stand density in the last millennium at the upper tree-line ecotone in the Polar Ural Mountains *Canadian J. For. Res.* **35** 2082–91
Mazepa V S and Devi N M 2007 Development of multistemmed life forms of Siberian larch as an indicator of climate change in the timberline ecotone of the Polar Urals *Russ. J. Ecol.* **38** 440–3
Mazepa V, Shiyatov S and Devi N 2011 Climate driven change of the stand age structure in the Polar Ural Mountains *Climate Change: Geophysical Foundations and Eco Logical Effects* (London: IntechOpen) pp 377–402
Meester R and Roy R 1996 *Continuum Percolation* (Cambridge: Cambridge University Press) (https://doi.org/10.1017/CBO9780511895357)
Moore I D, Grayson R B and Ladson A R 1991 Digital terrain modeling—a review of hydrological, geomorphological, and biological applications *Hydrol. Process.* **5** 3–30
Myers-smith I H *et al* 2011 Shrub expansion in tundra ecosystems: dynamics, impacts and research priorities *Environ. Res. Lett.* **6** 045509
Myers-smith I H *et al* 2015 Climate sensitivity of shrub growth across the tundra biome *Nat. Clim. Change* **5** 887–91
Myers-smith I H, Kerby J T, Phoenix G K, Bjerke J W, Epstein H E, Assmann J J, John C, Andreu-hayles L, Angers-blondin S and Beck P S 2020 Complexity revealed in the greening of the Arctic *Nat. Clim. Change* **10** 106–17
Paulsen J and Körner C 2014 A climate-based model to predict potential treeline position around the globe *Alp. Bot.* **124** 1–12
Pearson R G, Phillips S J, Loranty M M, Beck P S A, Damoulas T, Knight S J and Goetz S J 2013 Shifts in Arctic vegetation and associated feedbacks under climate change *Nat. Clim. Change* **3** 673–7
Plotkin J B, Chave J and Ashton P S 2002 Cluster analysis of spatial patterns in Malaysian tree species *Am. Nat.* **160** 629–44
Porter C *et al* 2018 ArcticDEM. V1 ed.: Harvard Dataverse (https://doi.org/10.7910/DVN/OHHUKH)
Ripley B D 1976 The second-order analysis of stationary point processes *J. Appl. Probab.* **13** 255–66
Sato H and Kobayashi H 2018 Topography controls the abundance of siberian larch forest *J. Geophys. Res.-Biogeosci.* **123** 106–16
Shiryaev A G, Moiseev P A, Peintner U, Devi N M, Kukarskih V V and Elsakov V V 2019 Arctic greening caused by warming contributes to compositional changes of mycobiota at the Polar Urals *Forests* **10** 1112
Shiyatov S G, Terent'ev M M and Fomin V V 2005 Spatiotemporal dynamics of forest-tundra communities in the polar urals *Russ. J. Ecol.* **36** 69–75
Shiyatov S G, Terent'ev M M, Fomin V V and Zimmermann N E 2007 Altitudinal and horizontal shifts of the upper boundaries of open and closed forests in the Polar Urals in the 20th century *Russ. J. Ecol.* **38** 223–7
Shiyatov S and Mazepa V 2011 Climate-driven dynamics of the forest-tundra vegetation in the Polar Ural Mountains *Contemp. Problem. Ecol.* **4** 758–68
Shiyatov S and Mazepa V 2015 Contemporary expansion of Siberian larch into the mountain tundra of the Polar Urals *Russ. J. Ecol.* **46** 495–502
Sturm M, Racine C and Tape K 2001 Climate change. Increasing shrub abundance in the Arctic *Nature* **411** 546–7
Sullivan P F, Ellison S B, Mcnown R W, Brownlee A H and Sveinbjornsson B 2015 Evidence of soil nutrient availability

as the proximate constraint on growth of treeline trees in northwest Alaska *Ecology* **96** 716–27
Tape K D, Gustine D D, Ruess R W, Adams L G and Clark J A 2016 Range expansion of moose in Arctic Alaska linked to warming and increased shrub habitat *PLoS One* **11** e0152636
Tape K, Sturm M and Racine C 2006 The evidence for shrub expansion in Northern Alaska and the Pan-Arctic *Glob. Change Biol.* **12** 686–702
Tily R and Brace C J 2006 A study of natural neighbour interpolation and its application to automotive engine test data *Proc. Inst. Mech. Eng.* D **220** 1003–17
Van Bogaert R, Haneca K, Hoogesteger J, Jonasson C, De Dapper M and Callaghan T V 2011 A century of tree line changes in sub-Arctic Sweden shows local and regional variability and only a minor influence of 20th century climate warming *J. Biogeogr.* **38** 907–21
Vavrus S J, Holland M M, Jahn A, Bailey D A and Blazey B A 2012 Twenty-first-century arctic climate change in CCSM4 *J. Clim.* **25** 2696–710
Walker D A *et al* 2005 The Circumpolar Arctic vegetation map *Journal of Vegetation Science* **16** 267–82
Walker M D *et al* 2006 Plant community responses to experimental warming across the tundra biome *Proc. Natl Acad. Sci. USA* **103** 1342–6
Wilmking M, Juday G P, Barber V A and Zald H S J 2004 Recent climate warming forces contrasting growth responses of white spruce at treeline in Alaska through temperature thresholds *Glob. Change Biol.* **10** 1724–36
Zeng H, Jia G and Forbes B 2013 Shifts in Arctic phenology in response to climate and anthropogenic factors as detected from multiple satellite time series *Environ. Res. Lett.* **8** 035036
Zevenbergen L W and Thorne C R 1987 Quantitative-analysis of land surface-topography *Earth Surf. Process. Landf.* **12** 47–56
Zhang W X, Miller P A, Smith B, Wania R, Koenigk T and Doscher R 2013 Tundra shrubification and tree-line advance amplify arctic climate warming: results from an individual-based dynamic vegetation model *Environ. Res. Lett.* **8** 10